Dynamic Finite Element Modelling of a Fall on the Hip

Nils Nyberg

2021

Master's Thesis in
Biomedical Engineering

Supervisors: Lorenzo Grassi, Hanna Isaksson, Joeri Kok

LUND
UNIVERSITY

Faculty of Engineering LTH
Department of Biomedical Engineering

1 Abstract

Assessing the risk of future femur fracture is an important step in preventing this serious and common injury. The current methods to predict the fracture risk are typically based on bone mineral density measurement, used as a surrogate for femoral strength. An alternative to this which has been shown to give more accurate information on the strength of a femur is subject specific finite element analysis, generally in a loading position that approximates a sideways fall since this is how most femur fractures occur.

Most such models are static or quasi-static, these provide an estimate of the force needed to fracture the femur under a constant or slowly increasing load. They do not however model the actual impacts under which the femur would break in a sideways fall and are thus limited in their ability to predict its behavior under such conditions. In this project a subject specific dynamic finite element modeling procedure solved with an explicit solver was developed. Models of 8 femurs from 22 to 88 year old women were created and the results of these models were evaluated. The meshes of these models were based on the geometry of the subjects bone found from CT-images and use element specific tangent stiffness and density which were also based on CT images of the femur. Additionally the models take into account the strain rate dependence of the stiffness of bone. The femur is given an initial velocity such that it hits a rigid surface.

The results of these models show good agreement with the results expected based on theory and previous tests of these femurs. Most femurs were predicted to fracture in the lateral femoral neck as expected when compared to previous quasi static loading tests of the same femurs. The impact forces at which the femurs would be expected to fracture during an impact were predicted based on the forces under which they fractured during quasi static loading and an experimental relationship between these. Comparing these expected fracture forces to the force at time of fracture from the simulations showed good agreement between the two. The major differences between the expected fracture forces and the ones predicted by the dynamic simulations were occurred in models of femurs much weaker than those used in the experimental study which found the relationship between the fracture forces for quasi-static and impact situations. The results seem promising for future work, such as adding soft tissue to the model, since they do appear to accurately capture the mechanical properties of each femur.

2 Acknowledgements

I would like to thank my supervisors Lorenzo Grassi, Joeri Kok, and Hanna Isaksson for all their help during this project. Their being easily available to answer questions and providing help during the project despite the COVID-19 pandemic was invaluable.

I would also like to thank Björn Lundin for helping to solve the problem with element specific density in Abaqus/Explicit.

3 List of Abbreviations

aBMD - Areal Bone Mineral Density
BMD - Bone Mineral Density
CT - Computed Tomography
FE - Finite Element
-

4 Introduction

Broken or fractured femurs are a common issue in the modern world, especially among the elderly. In the year 2000 there were an estimated 1.6 million hip fractures in the world [1] and that number has been predicted to increase to 4.5 million by 2050 [2]. This is a serious problem as hip fractures have serious consequences for the patient, as many as 20% of whom die within a year of the fracture. This creates not only a great deal of suffering but also costs large amounts of money to pay for the often extensive medical treatment needed by the patient. One of the biggest causes of a fractured femur is falls on the side from a standing position, especially when the person falling has osteoporosis, i.e. weak bones [3] which is a problem common among the elderly.

Being able to determine whether someone is at risk of a hip fracture might help prevent fractures. Fractures can be prevented by prescribing medicine or exercise to strengthen the bone, or by trying to prevent the patient from falling in the first place, for example by exercises to improve their balance. It could also possibly make testing of things such medicines easier and faster by allowing the results to be evaluated numerically.

Currently areal bone mineral density (aBMD), possibly in conjunction with other information on the subject, is used to assess the risks of fracture. This method is limited in that it does not take the geometry of the patients bones into consideration. To solve this, one can make finite element (FE) models generated from CT scans of individual patients, with the models geometry based on the image's shape and the stiffness on the image's brightness. This is a promising alternative currently being developed and has the potential to generate better results. One example of such is created by Grassi et al [4]. It uses CT images to generate a subject specific quasi-static FE models. These models have material properties and geometry matching the bone in question. Displacements are then applied to the femur to find the force at which it fractures. This gives information about the strength of the bone but does not model an actual fall in which a femur would fracture since it does not model the femurs impact with the ground. This model is solved with an implicit solver [4,5].

Falls are dynamic situations so to create a more true to life model a sideways fall might require dynamic analysis. This is because in dynamic analysis the movement and deformation of a structure over time is modeled. This allows one to model situations such as an impact. In static analysis however this cannot be done

since such analysis only models the final result of exposing the structure to a constant load over a long time. Quasi-static analysis is similar to static. In quasi static analysis changes over time are modeled under the assumption that they are slow enough that all accelerations can be approximated to be zero making inertia irrelevant. This allows the bones strength to be estimated by predicting what constant force it will break under but does not allow the creation of a hypothetical fall situation and checking whether the bone will break or not. An example of a dynamic FE modeling scheme for femurs has been created by Fleps et al [6]. Further, in dynamic analyses solving the problem explicitly rather than implicitly is often preferable for performance reasons, especially when contact must be considered.

4.1 Aim

The aim of this project is to create a subject specific dynamic FE modeling procedure for a femur impact with the ground simulating a sideways fall on the hip. These simulations will be performed using explicit time integration. The purpose is to investigate the methods viability for predicting hip strength and fall outcomes, which may be useful in predicting the risk of hip fracture.

4.2 Study Design

The project consisted of first creating the aforementioned dynamic subject specific explicit finite element modeling procedure of the femur. This process consisted largely of coding to change the quasi-static modeling procedure created by Grassi et al [4] into a dynamic explicit one. It was then tested on CT-scans from a number of bones from a previous study [22]. The results of these simulations were then evaluated and, compared to previous results of quasi-static tests for these femurs by Kok et al and to existing knowledge.

5 Theory

5.1 Anatomy of the Femur

The femur is the largest bone in the human body. It is the bone of the upper part of the leg where the head of the femur connects to the pelvis and its distal end connects to the knee (Fig. 1 a)). [9]

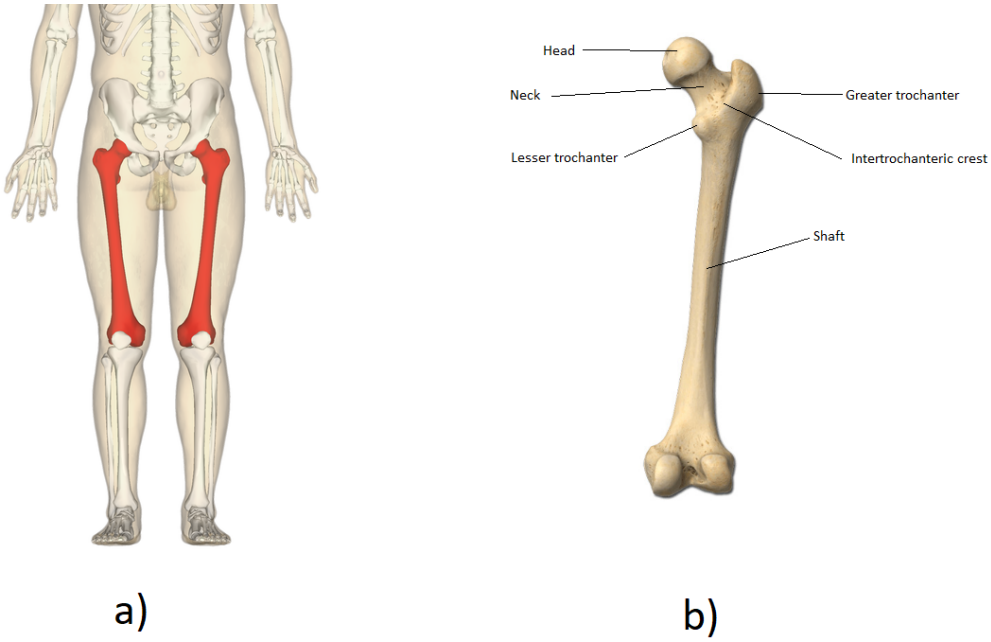

Figure 1: a) Anterior view of the lower part of a skeleton with the femurs highlighted in red [8]. b) Posterior view of the femur with parts of interest identified.

In the proximal femur, the head, neck and trochanters are found (figure 1 b)) [15]. The two main types of hip fractures occur in the proximal femur on the neck or trochanters, these are referred to as cervical or trochanteric fractures respectively [21].

5.2 Osteoporosis and femur fracture

Fractures in the proximal femur are common and serious injuries that often afflict elderly people with osteoporosis. Femur fractures have serious consequences for the patients with about 10% dying within 3 months of the fracture and about 20% being dead after a year. A year after the fracture about half of the patients report some form of reduced mobility. Almost all hip fractures are caused by a low energy accident, such as the patient falling over in their house [21].

Osteoporosis is diagnosed by measuring the bone mineral density (abbreviated as BMD), that is the mass of bone per area or volume generally measured in g/cm^2 or g/cm^3 respectively. These measurements are generally made in the femoral neck using x-ray technology, generally dual energy x-ray absorptiometry. A person is considered osteoporotic if their BMD is 2.5 standard deviations below the average for young women [3]. There is however much information indicating that BMD and osteoporosis diagnosed through BMD is an insufficient surrogate for the mechanical properties of the bone in determining the strength of the bone. This data about bone strength is used to asses fracture risk. A BMD indicating osteoporosis in the femur indicates a high risk of a hip fracture, however many fractures occur in people with BMD which does not indicate osteoporosis. As many as 73% of fractures (not just hip fractures in this case) in women occur in patients without osteoporosis [12]. Factors other than BMD are important to the mechanical properties of bone, one example of such a property is the bone's geometry [13]. It has been shown that QCT based FE analysis outpreforms BMD as a way to predict the failure load of a femur in a sideways fall configuration [14].

5.3 Kinematics of a Sideways Fall on the Hip

During a sideways fall on the hip from a standing position the impact velocity of the trochanter is generally around 3.1 m/s [6].

The soft tissue around the greater trochanter can absorb large amounts of energy during impact and reduce the peak force experienced by the femur, the thicker the soft tissue the greater this effect. One study has found that for every millimeter of thickness of the soft tissue around the greater trochanter the peak impact force decreased by about 70 N and the energy absorbed by the soft tissue increased by 17 J per mm [23].

The fracture forces involved in a fall on the hip and quasi-static loading in a sideways fall configuration have been compared in an experimental study by Jazinizadeh

et al [25]. This was done by taking the right and left femurs from different cadavers, both genders ages 53 to 73 with aBMD between 759 and 1105 mg/cm^2, and placing one in a quasi-static sideways fall loading situation with a deformation rate of 0.017 mm/s and the other in a dynamic impact situation with an impact velocity 3.0 m/s. The fracture load for quasi-static loading was on average 3637 ± 863 N with the fracture load for the impact loading being on average 7326 ± 771 N. Equation 1, where F_{imp} and F_{qs} are the fracture loads for the impact and quasi-static tests respectively, is a relation with moderate correlation observed between the two fracture loads. It was found that fracture patterns were similar for both the quasi-static and impact tests [25].

$$F_{imp} = 0.61F_{qs} + 5173N \tag{1}$$

5.4 Mechanical Properties of Bone for FE Model

Bone is a rigid material that makes up the skeleton. Bone can be categorized into two types: cortical bone, and trabecular bone. Cortical bone is dense with between 85 to 95$\%$ of its volume being made up of bone. Cortical bone is like a shell found on the outside of long bones like the femur, it is thicker on the shaft than at the ends of the bones. Cortical bone in the femur can have a tangent modulus of up to 21800 MPa under longitudinal loading. Under transverse loading its much lower at, between 12500 and 3270 MPa [26]. Trabecular bone is more porous than cortical bone and can has between 60 to 5 $\%$ of its volume made up of bone and has a much lower tangent modulus than cortical bone. Trabecular bone makes up the inside of bones like the femur within the shell of cortical bone. Once strained to a certain point bone will yield permanently reducing its stiffness but before reaching that point it is linearly elastic for a constant strain rate. Bone is viscoelastic, meaning its tangent modulus increases with faster deformations, and anisotropic, meaning its mechanical properties are direction dependent [26].

In creating the subject specific FE model it is important to find the material properties of the bone, such as density and stiffness, in different parts of the femur. This allows the model to take into account things such as local weak spots in the bone.

It is possible to find the density of bone from QCT images which is done in two steps. First the CT number for the piece of bone considered is converted to QCT-density, ρ_{QCT}, through comparison to phantoms (pieces of material similar to

bone with known densities which are scanned alongside the sample). ρ_{QCT} can be converted to ash density, ρ_{ash}, which is the density of the minerals in the bone, i.e. the density of what would remain after the bone is burned. Calibration studies have found that the relationship between ρ_{QCT} and ρ_{ash} is:

$$\rho_{ash} = 0.079 + 0.877\rho_{QCT} \tag{2}$$

Ash density does not take into account the mass of the non-mineral components of the bone. Therefore apparent density, ρ_{app}, is sometimes used instead. Apparent density is the mass of the undried bone divided by its total volume with pores included. When a conversion between these are needed ρ_{ash} can be converted to ρ_{app} according to the empirically found equation 3 below. [19]

$$\rho_{app} = \frac{\rho_{ash}}{0.6} = \frac{0.079 + 0.877\rho_{QCT}}{0.6} \tag{3}$$

The relationship between the apparent density of trabecular bone in the femoral neck (trabecular bone makes up most of the femoral neck) has been empirically determined to be

$$E = 6850\rho_{app}^{1.49} \tag{4}$$

where E is the tangent modulus in GPa and ρ_{app} is the apparent density in $\frac{g}{cm^3}$ [20].

The stiffness of bone is dependent on the strain rate, i.e. the time derivative of the strain, during deformation. The tangent modulus of the bone is at a time proportional to the strain rate to the power of 0.06 or 0.05 [16]. Expressed as an equation

$$E_{eff} = E(b\frac{\partial\epsilon}{\partial t})^{0.06} \tag{5}$$

Where E_{eff} is the effective tangent modulus at the time, b is some constant and ϵ is the strain. Yield and fracture properties of bone are also show strain rate dependence. Cortical bone generally becomes more brittle, and thus yields and fractures at lower strains, with higher strain rates although this also depends on whether the strains are compressive or tensile [27].

When strains in bone get high enough, but before it fractures, it will yield. When it yields the tangent Modulus of the bone decreases greatly. Depending on whether the strains are tensile or compressive this yield strain will be different, about 0.0073 and 0.0104 [18]. By averaging post yield strain values from another study the post yield tangent modulus can be estimated to be about 5.5% of the pre-yield stiffness [17].

When tested to failure one discovers that bone from the shaft of the human femur fractures at different strains for tension and compression. Working out the average failure strain for human bone for tension and compression one ends up with 0.027421 and 0.0211 respectively [17].

5.5 Implicit and Explicit solvers in the Finite Element Method

The finite element method is a numerical method for solving partial differential equations that describe some physical phenomena, such as movement and deformation, in 2D or 3D space by dividing it into a number of elements made up of individual nodes. Using these elements and taking into account loads and boundary conditions one can then create a linear equation system to solve for the displacement of the nodes, and/or other values depending on what the problem is.

In static finite element analysis the equation system is

$$KU = R \tag{6}$$

where K is the stiffness matrix created from the tangent modulus of the elements, R is the load vector created from the loads on the nodes and U is the displacements of the nodes. When simulating dynamic situations however the acceleration and velocity must be taken into account in this equilibrium equation according to

$$M{}^t\ddot{U} + C{}^t\dot{U} + K{}^tU = {}^tR \tag{7}$$

where M is the mass matrix created from the density of the elements, ${}^t\ddot{U}$ is the acceleration of the nodes at time t, C is the damping matrix, ${}^t\dot{U}$ is the velocity of the nodes at time t, ${}^tU$ is the displacement of the nodes at time t and ${}^tR$ is the load at time t. Solving this involves finding ${}^{t+\Delta t}U$, ${}^{t+\Delta t}\dot{U}$, and ${}^{t+\Delta t}\ddot{U}$ given knowledge of their value at t and possibly earlier points in time. Finding this solution can be done either explicitly or implicitly which is referred to as taking a time step of size Δt.

Implicit methods find a solution to the equilibrium equation 7 at time $t + \Delta t$, and one must solve equations of the form $F({}^{t+\Delta t}U, {}^{t+\Delta t}\dot{U}, {}^{t+\Delta t}\ddot{U}) = {}^{t+\Delta t}R$, where F is a function dependent on which method is used. This form of time integration has good stability and one can thus pick large value for Δt. However implicit methods can take a long time to solve since the solution will inevitably involve finding the solution of some linear equation system.

Explicit methods on the other hand have the form ${}^{t+\Delta t}U = F({}^{t}U, {}^{t}\dot{U}, {}^{t}\ddot{U})$. One example of such is the central-difference method. Here one uses the central difference method to approximate ${}^{t}\dot{U}$ and ${}^{t}\ddot{U}$ using the central difference approximation:

$$ {}^{t}\dot{U} = \frac{1}{2\Delta t}(-{}^{t-\Delta t}U + {}^{t+\Delta t}U) \tag{8} $$

$$ {}^{t}\ddot{U} = \frac{1}{\Delta t^2}({}^{t-\Delta t}U - 2{}^{t}U + {}^{t+\Delta t}U) \tag{9} $$

Inserting this into equation 7 and assuming $C = 0$ one ends up with

$$ {}^{t+\Delta t}\ddot{U} = \Delta t^2 M^{-1}({}^{t}R - K{}^{t}U) + 2{}^{t}U - {}^{t-\Delta t}U \tag{10} $$

This can be calculated very swiftly assuming M is a diagonal matrix. This form of time integration is however only conditionally stable which means Δt needs to be quite small and many steps are needed [11].

Since explicit solvers are only conditionally stable the time-step size must be chosen carefully. The time step should be small enough to ensure stability but for performance purposes it should be as large as possible. In an isotropic material an approximation of a good stable step size can be found according to

$$ \Delta t \approx a \cdot L_{min}\sqrt{\frac{\rho(1+\nu)(1-2\nu)}{E(1-\nu)}} \tag{11} $$

where L_{min} is the smallest dimension of the element and a is some constant smaller than 1 to ensure convergence. Thus the stable time step is dependent on the mesh, tangent modulus and density [10].

6 Methods

6.1 Material

For this project CT-images of 12 human proximal femurs from human cadavers were available. These femurs came from women who were between the ages of 22 and 88 at the time of their deaths with a median age of 70.5 year. These femurs had also previously been tested in a sideways fall position where they were loaded through an enforced displacement of 5 mm/s on the femoral head with the greater trochanter fixed in the loading direction until they fractured. A summary of these femurs, referred to by numbers between 45 and 60, and some of the data from these tests can be found in table 1. The fractures of the femurs, with a single exception, started on the lateral side of the femoral neck close to the greater trochanter [22].

These CT-images were previously used to create quasi-static models of the above mentioned tests by Kok et al (2021). This model predicted the forces and locations of the fractures well when the surface elements were given a minimum tangent modulus of 2.5 GPa. When this was not done the model sometimes erroneously predicted fractures close to the femoral head, likely due to the cortical bone being particularly thin there causing problems in estimating the density of these elements due to a partial volume effect. The surface geometries for models of these femurs created through segmentation of the CT-images of the femurs by Kok et al were also available [5].

All simulations in this project were preformed on a Windows computer with a 3.30GHz processor. For context the quasi-static model took about 3 hours to run on the same computer.

Table 1: The locations of the fractures for all the femurs, along with the force at the time of fracture and the energy required to fracture them. The abbreviations in the last column mean pertrochanteric (PT), basicervical (BC), intertrochanteric (IT), and midcervical (MC).

Femur	Age in Years	Weight (kg)	aBMD (g/cm^2)	Peak Force (N)	Energy to fracture (Nm)	Fracture Location
45	70	120	0.818	3975	8.358	PT
46	83	56	0.670	2383	3.728	PT
47	68	62	0.989	4451	8.876	BC
49	85	48	0.429	1515	1.705	PT
50	22	96	0.971	5477	23.250	BC
51	67	98	1.053	4531	8.895	IT
52	68	NA	0.643	4246	12.642	BC
53	88	NA	0.739	4706	12.938	BC
54	81	67	0.550	2520	3.443	PT
55	80	77	0.736	3523	6.259	BC
57	71	64	0.830	4718	7.437	MC
60	59	55	0.917	5325	16.901	PT

6.2 Modeling

The project largely consisted of adapting quasi-static models and modeling procedures that could simulate the femur under a deformation load in a sideways fall position [4,5] to instead simulate a dynamic fall, adding things such as density and contact to the model. Additionally the time integration was changed from implicit to explicit. The sections below describe the final models and the motivation for the decisions made when making it.

Abaqus Explicit, which was used in this project, is a finite element modeling software for creating explicit dynamic finite element models. Abaqus Explicit uses the finite difference method for time integration when solving these models. The quasi-static model was solved in Abaqus Standard.

The model was implemented in Abaqus Explicit where the tangent modulus of the material, was implemented within the user subroutine vusdfld. This subrou-

tine allows material properties of individual elements in the mesh to be modified during the simulation between time steps. This subroutine is run for each element following each time step.

6.2.1 The Mesh

The meshes for the femurs were generated automatically using Hypermesh from geometric data for the twelve bones previously used by Kok et al [5]. The elements were second order tetrahedral elements with an approximate side of 3mm. This represents an increase of the element size compared to what was used in the quasi-static model, see figure 2 for a comparison. This was needed to keep the simulation time from reasonable. Usage of a finer mesh was attempted but due to finer meshes necessitating shorter time steps, see equation 11, and containing more elements this took too much computational time, several days for each simulation. Usage of a coarser mesh reduced the stable time step from approximately $7.9 \cdot 10^{-9}$ to $1.4 \cdot 10^{-8}$ seconds for bone 54. It also reduced the number of elements in the mesh from about 157924 to only 32381 which reduces the work required for each time step since it reduces the size of the matrices in equation 10 and reduces the number of times the vusdfld subroutine needs to be run.

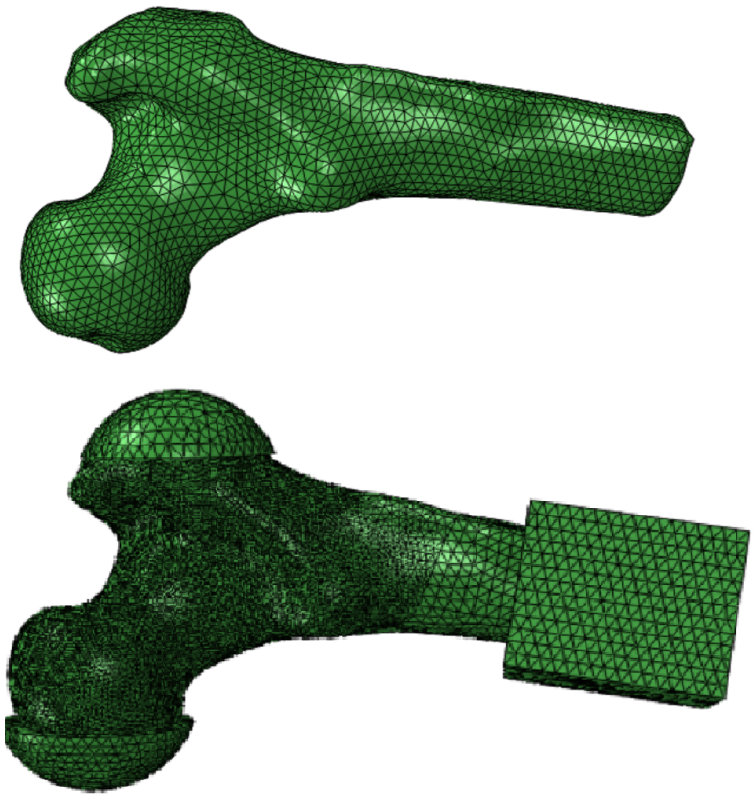

Figure 2: Comparison between the element sizes in the explicit dynamic model (above) and the quasi-static model (below) for femur 54. The cups on the femoral head, greater trochanter, and the distal end of the femur are components of the experimental setup simulated by the quasi-static model.

6.2.2 Material Model

In the material model each element in the mesh was assigned an apparent density which was found by comparing the mesh to the CT scans from which it was made using Bonemat version 3 (www.bonemat.org) [24]. The elements were then assigned an initial tangent modulus, E_0, based on the apparent density using equation 4. During the simulation the stiffness is updated based on the strain rate according to equation 5. The constant b in equation 5 was set to 0.005 s since that is the strain rate at which the relationship between the apparent density, ρ_{app}, and the tangent modulus, E, was derived [20]. The strain rate correction factor was not allowed to go below 1. If the strain in the element exceeded the yield strain, 0.0073

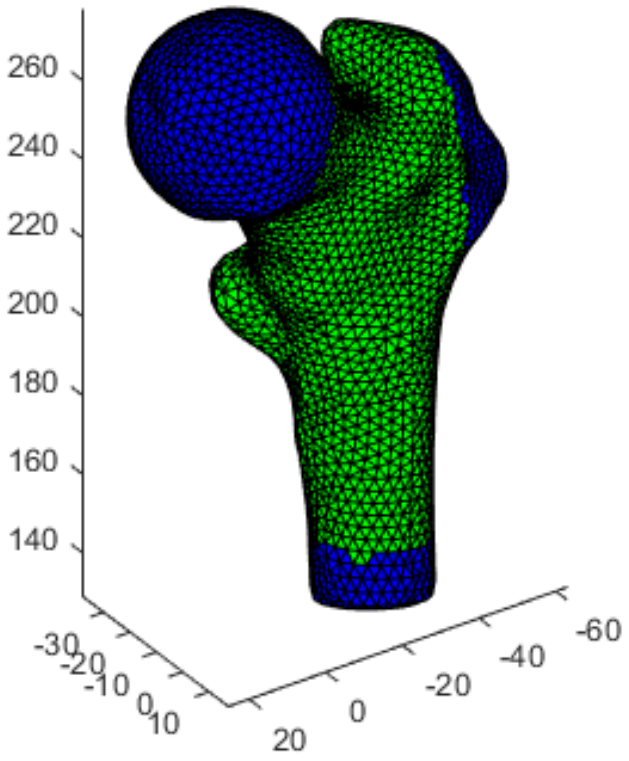

Figure 3: Example of the mesh of the proximal femur, where the elements that were allowed to fracture are green and the elements that could not fracture are blue. The femur is number 52.

and 0.0104 for tensile or compressive strain respectively, the tangent modulus was multiplied by 0.055 from then on unless the element later fractured. After the element fractured, as determined by it reaching the tensile or compressive strains 0.027421 or 0.0211 respectively, the tangent modulus was set to 5 MPa. While all elements could yield, only surface elements could fracture. Additionally surface elements close to the contact surface on the greater trochanter or on the head of the femur were not allowed to fracture since these are unlikely outcomes of a sideways fall which may otherwise happen in the model due to erroneous strain measurements close to the contact and mass areas, see figure 3 for an example.

The element specific density needed to be implemented using element specific

nonstructural mass since the ways in which other material properties can be assigned at an element level in Abaqus/Explicit, such a distribution or vusdfld subroutine, do not function for density. Nonstructural mass in Abaqus allows additional mass to be added to parts of the model. It is ordinarily meant to model things that contribute mass to the model but has no other mechanical impact, for example the mass contributed to a plane by the paint. All other element specific behavior, e.g. tangent modulus and which elements have fractured, can and were handled in the vusdfld subroutine. Vusdfld being different from the implicit equivalent usdfld the creation of this subroutine required significant amounts of coding effort since many of the previous solutions did not carry over. Examples of this include different or unavailable functions, the different structures of the function and the aforementioned difficulty with element specific mass.

6.2.3 Initial and Boundary Conditions

The femur was initially placed in a configuration commonly used for sideways falls, 10^o adduction, 15^o internal rotation. This configuration has been used to represent sideways falls for a long time, it is also the configuration under which the femurs modeled in this project have previously been tested and modeled [22]. The femur was placed with its lowest point in the x direction, which was at the lateral end of the greater trochanter, 2 mm above a fixed rigid plane with which if could make contact, see figure 4.

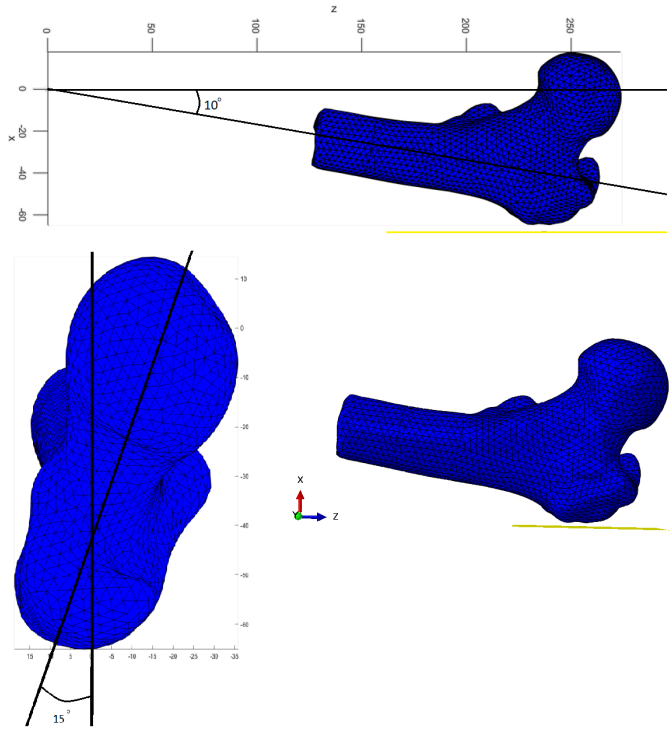

Figure 4: An example of the initial placement of the femur (blue) and rigid plane (yellow) in the model.

The nodes at the distal end of the femur were constrained to only rotate with respect to the y axis around a constraint node -126.5 mm away from them in the z direction. This is a guess at the distance between those nodes and the knee previously used in Kok et al's quasi static models [5].

The femur started the simulation with a velocity of $-3.1m/s$ in the x-direction, see Kinematics of a Sideways Fall on the Hip in the theory section. The model was not subject to any other initial velocities or gravity.

The mass to represent the body was added as increased density to surface elements of the femoral head, see figure 5. For the subjects who had no known body mass a mass of 68 kg was assumed since this is the average weight for women in Sweden.

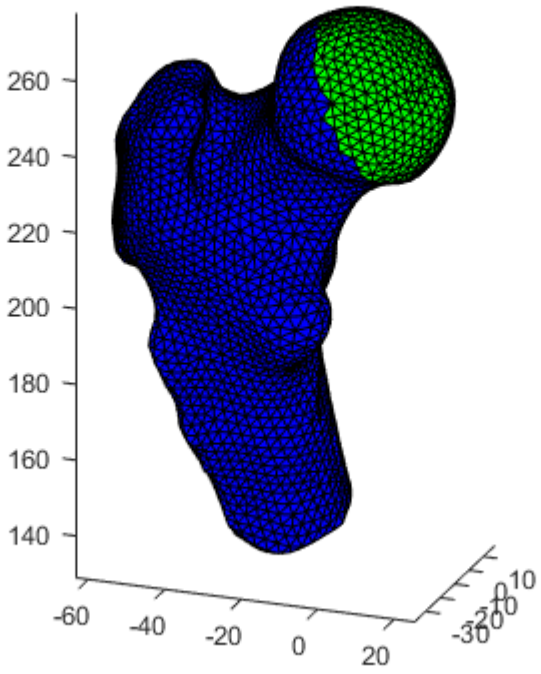

Figure 5: Example of mass elements in femur 52. The green surface elements are the ones to which the mass of the body was added.

6.3 Testing

In first tests models were created for ten femurs according to the above procedure with the mass selected as the entire mass of the body. The simulation was stopped 1000 time steps after the time step when the first fracture occurred in an element. This stopping criterion was chosen because the goal of these first simulations was to investigate if the femurs would fracture and under what circumstances, so there was little reason to continue on far beyond the initial fracture. 1000 time steps represented only about 1% of the total simulation time. The output from these simulations were the displacements and velocities of the nodes at evenly spaced time points in the simulation, variables derived from these displacements such as strain, the contact force over time, multiple forms of energy over time, and which elements fractured and when this happened. Simulations for femurs 57 and 60 were not run due to time constraints.

These simulations stopped before the peak force was reached. Thus tests where the simulation would stop at a later point were run to find the peak force. These tests were identical to the first set of tests except they stopped after $2.0 \cdot 10^{-3}$ s rather than a certain number of time steps after the first fracture. This amount of time was chosen since it could be seen that this was sufficient time to capture the peak contact force of the impact from test simulations that were not included here. The types of output available from these simulations were the same as above.

A third set of simulations were run with femurs 45, 49, 50, and 53 with the mass of the body set to 1 kg.

This mass was chosen because with an initial velocity of 3.1 m/s it results in an approximate kinetic energy of 4.805 Nm. This is about half the average work previously needed to fracture these femurs in a similar position, see table 1. The reason femurs 45 and 53 were selected was because they represented one slightly weaker than average and one slightly stronger than average femur from the set. Femurs 49 and 50 were selected because they were the weakest and strongest of the femurs of the set. This selection was based on the amount of energy it previously took to fracture them in the quasi-static loading study [22], see table 1 for these energies. The kinetic energy of the fall was calculated according to $\frac{3.1^2 \cdot 1}{2} Nm = 4.805 Nm$, the mass of the femur was neglected since they tended to weigh only about 0.10 to 0.13 kg. The types of output available from these simulations were the same as above.

7 Results

Due to errors made in the creation of the meshes femurs 51 and 52 where placed with an internal rotation of -15^o rather than 15^o. The results of these simulations have not been included in this section.

In simulating the 8 models with the full mass applied to the head of the femur all of the modeled bones fractured, the location of the fracture and the force at the time of fracture, i.e. the fracture force, can be seen in table 2. The number of the elements capable of fracturing which had fractured 1000 time steps after can also be seen there. Examining the fracture locations, after these 1000 steps one finds that fractures generally occurred in one of two places, the back of the femoral head or close to the greater trochanther, see figures 6-7.

The femurs that were stronger during quasi static testing also had higher contact forces at time of fracture as can be seen by comparing table 1 to 2. For example femur 49 and 50, the strongest and weakest femurs in the set based on the tests, were also predicted to fracture at the lowest and highest force respectively by this model.

Table 2: The locations of the fractures for all the femurs but 51, 52, 57 and 60 along with the force at the time of fracture.

Femur	Location of Fracture	Contact force at time of fracture (N)	Amount of the elements able to fracture fractured (%)
45	Base of femoral head	7999	0.00293
46	Close to the greater trochanter	5027	0.01758
47	Base of femoral head	8820	0.00677
49	Base of femoral head	3889	0.00609
50	Close to the greater trochanter	9208	0.00663
53	Base of femoral head	7859	0.04244
54	Close to the greater trochanter	4800	0.00309
55	Base of femoral head	6604	0.00680

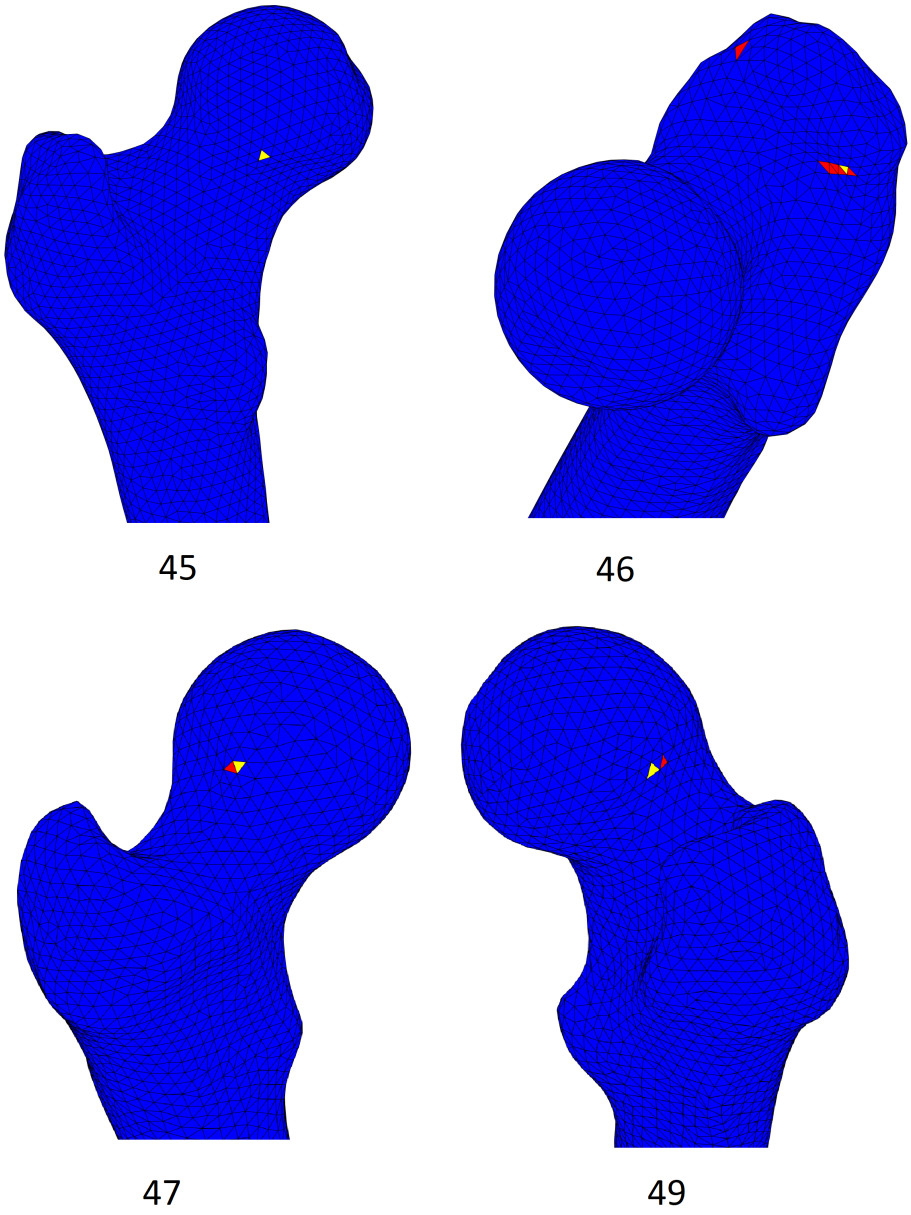

Figure 6: The fractured elements within the first 1000 time steps of the initial fracture in femurs 45 to 49. The initially fractured element in yellow and the other fractured elements in red.

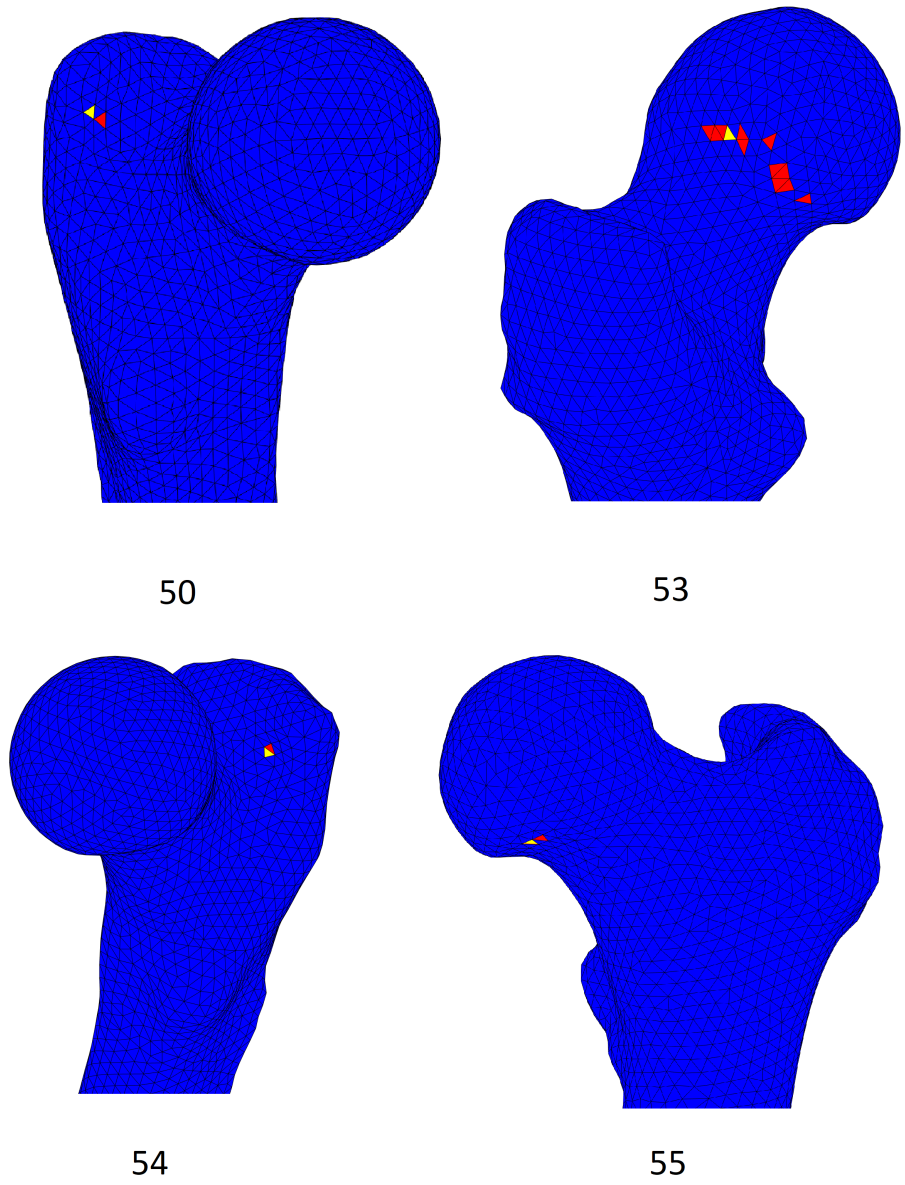

Figure 7: The fractured elements within the first 1000 time steps of the initial fracture in femurs 50 to 55. The initially fractured element in yellow and the other fractured elements in red.

The size and distribution of the highest principal logarithmic strain in femur 49 can be seen in figure 8. The strains are largest in the femoral neck and on the greater trochanter where it is in contact with the plane. The strain is largest on a line on the distal femoral neck close to the head, the fact that the fracture did not occur her is likely that the elements so close to the body mass elements weren't fracturble.

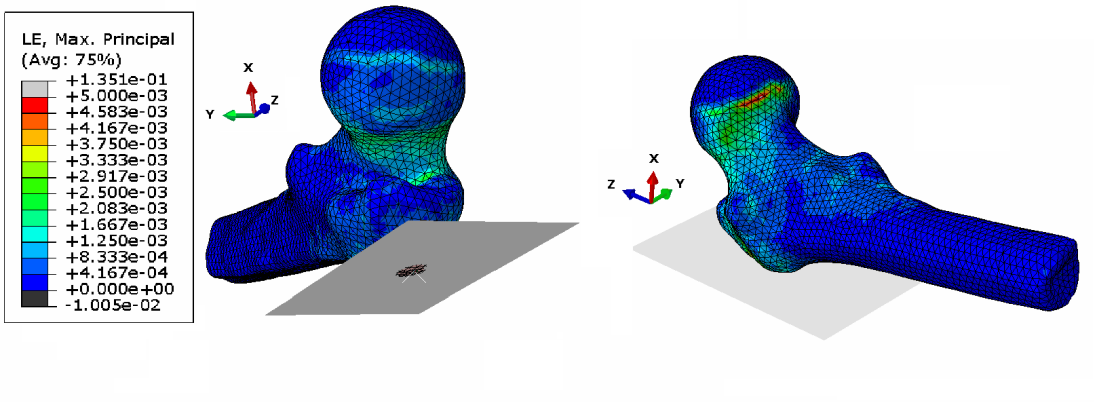

Figure 8: Strain distribution in femur 49 at time $1.0 \cdot 10^{-3}$ after the start off the simulation, before the fracture but after contact with the plane.

Overall the first simulations took between 5 and 9.3 hours to finish and had stable time steps of between about $1.0 \cdot 10^{-8}s$ and $1.7 \cdot 10^{-8}s$ before contact with the plane. After contact with the plane there was a slight decrease in the stable time step size as determined by Abaqus.

The longer simulations to find the peak force were sometimes aborted before the contact force could reach its peak due to the ratio of deformation speed to wave speed exceeding 1. Deformations speed exceeding the wave speed in an element is an error that occurs when the deformation speed is too large for a mesh with elements of the present size to handle at the current time step. This generally happened either close to fractured elements or on the femoral neck close to the head. Thus the peak force could not be identified with certainty in all simulations. The highest contact force from these simulations, and whether the simulation aborted due to deformation speed larger than wave speed before the contact force had reached its peak can be found in table 3. This table also contains the energy of the fall which exceeds the work needed to fracture the femur in the quasi static tests by more than an order of magnitude for all the femurs. Since the femur starts

the simulation undeformed and without potential energy due to the lack of gravity in the model, the total energy of the system is the same as the initial kinetic energy. Since the mass and initial velocity involved is the same as for the first tests, this energy would be the same for the first tests. Plots of force over time in these simulations can be found in figure 9.

Table 3: The peak contact force for the longer simulations and whether the simulation was aborted too early to find the peak force with any certainty early due to the ratio of deformation speed to wave speed exceeding 1. The time from first contact to the peak force is also included.

Femur	Peak force (N)	Aborted early	Total energy (Nm)	Time from contact to peak (ms)
45	10618	no	577	0.9014
46	6030	no	270	0.7167
47	10522	yes	299	0.7608
49	4649	no	231	0.10432
50	11335	no	462	0.7789
53	8875	no	327	0.5581
54	6387	yes	323	0.9281
55	7714	no	371	0.9149

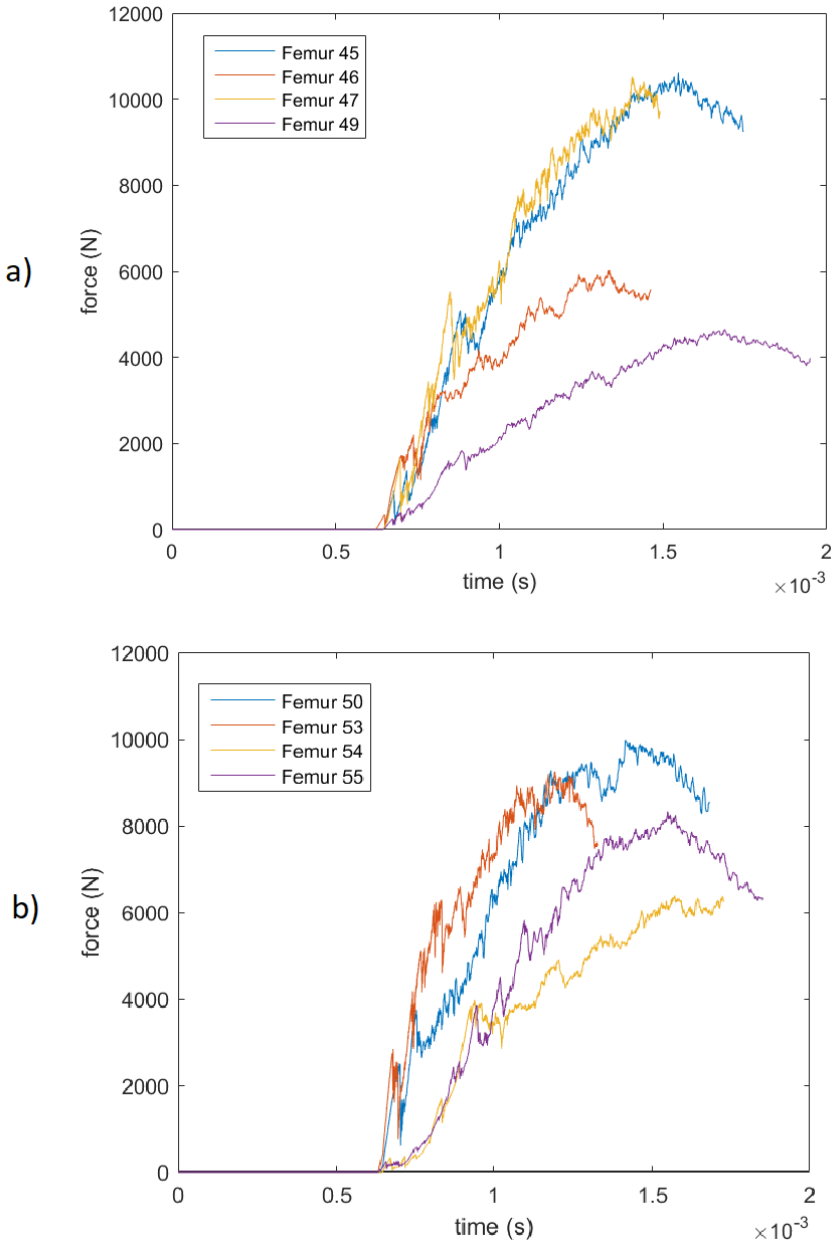

Figure 9: a) Contact force between the rigid fixed plane and the femur in the simulations of femurs 45, 46, 47 and 49. The horizontal axis is time in s and vertical is force in N.
b) Contact force between the rigid fixed plane and the femur in the simulations of femurs 51, 52, 53, 54, and 55. The horizontal axis is time in s and vertical is force in N.

Visualizations of the principal strain during the longer simulations for femurs 49, 50 and 53 around both the approximate time of fracture and peak force are found in figures 10 to 15. Here one can see that the strain is generally largest in the femoral neck. While hard to see in the figures high strains were also observed in the contact area. Strains later generally become larger in proportion to the rest of the bone in the areas where fractures occurred as can be seen in the figures showing strains around the peak force.

Fracture data for the whole simulation rather than just the first 1000 steps from the initial fracture shows that for three of the five femurs predicted to fracture by the femoral head fractures later also occurred on the lateral femoral neck. The full fracture locations for these bones can be seen in figure 18.

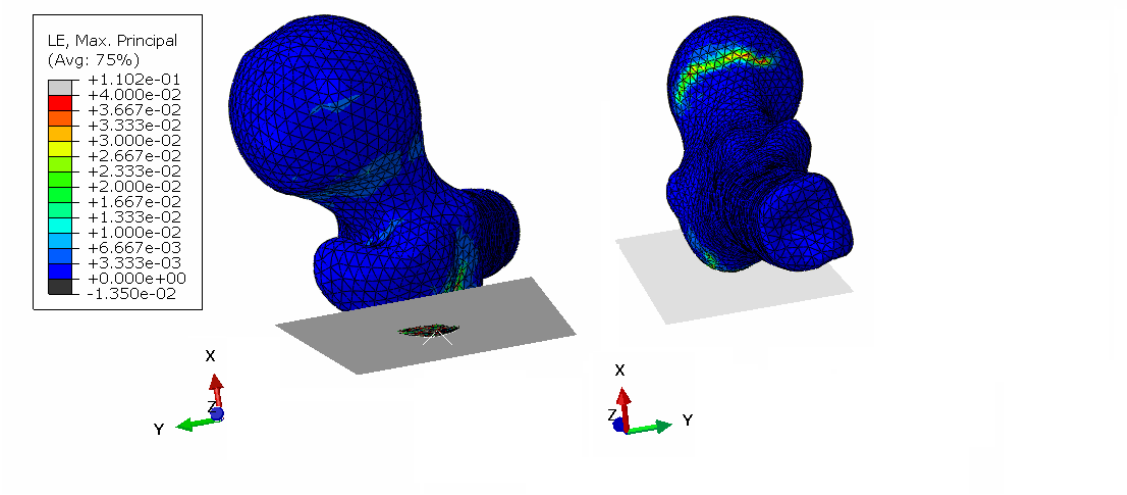

Figure 10: Strain distribution in femur 49 close to the time of the first fracture. Femur 49 is the weakest in the set.

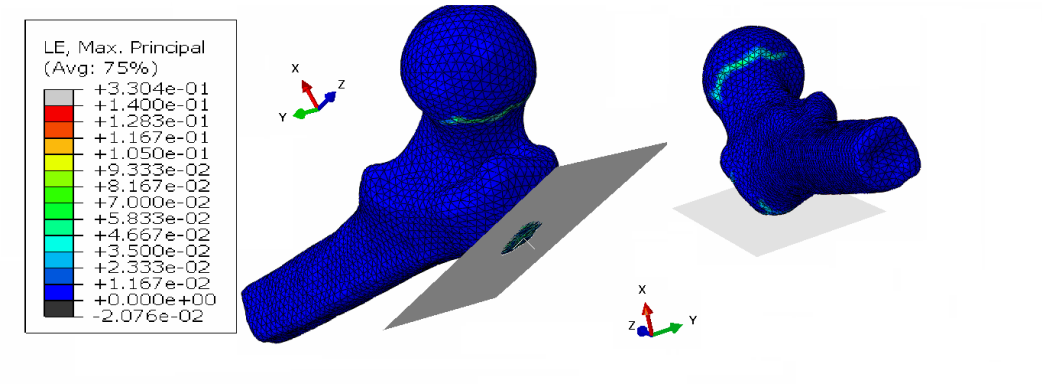

Figure 11: Strain distribution in femur 49 close to the time of the peak force was reached. Femur 49 is the weakest in the set.

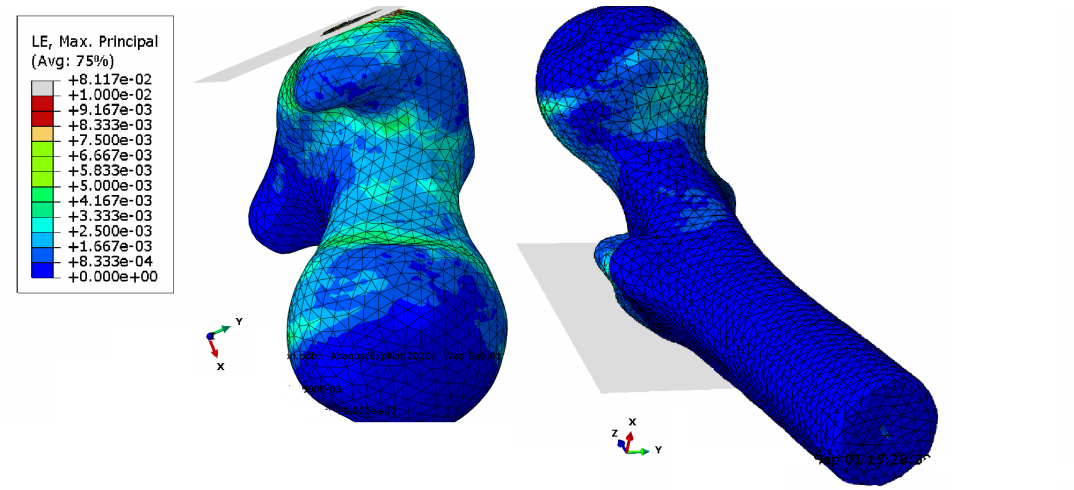

Figure 12: Strain distribution in femur 50 close to the time of the first fracture. Femur 50 is the strongest in the set.

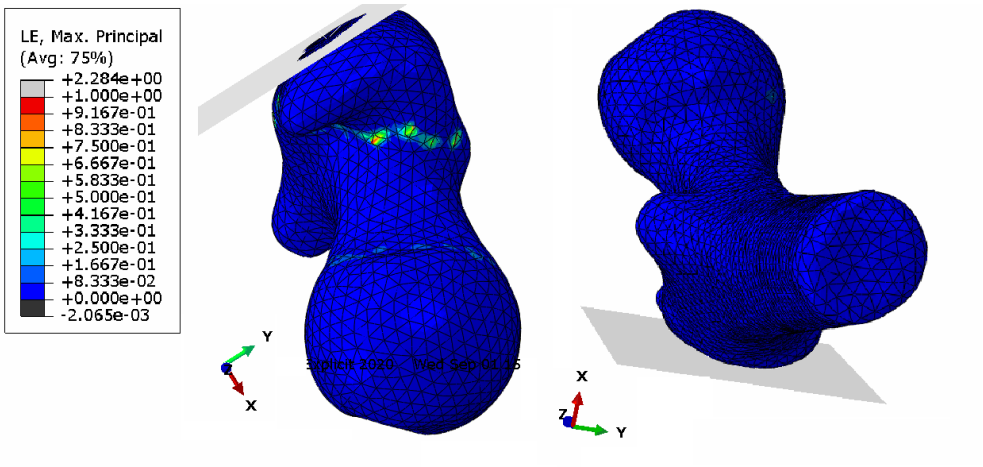

Figure 13: Strain distribution in femur 50 close to the time of the peak force was reached. Femur 50 is the strongest in the set.

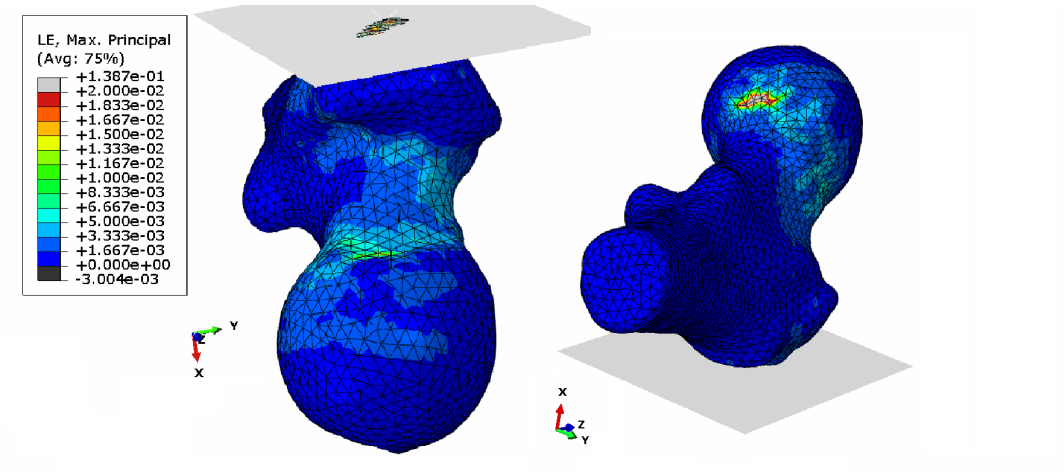

Figure 14: Strain distribution in femur 53 close to the time of the first fracture. Femur 53 is an average bone in the set.

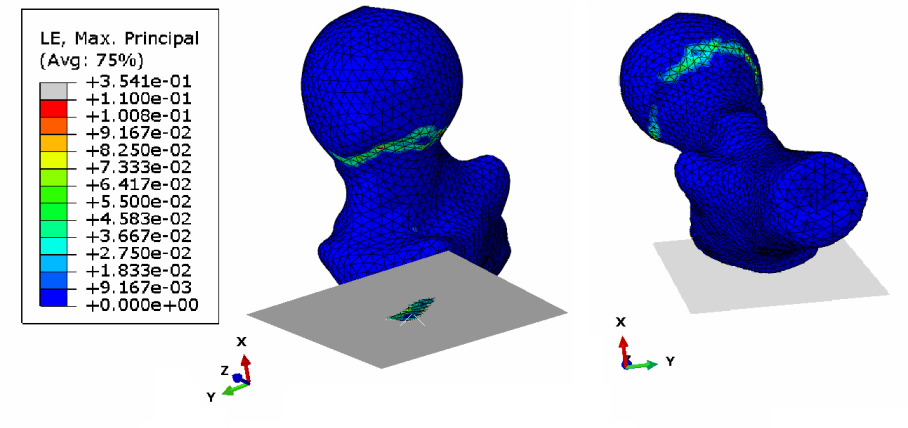

Figure 15: Strain distribution in femur 53 close to the time of the peak force was reached. Femur 53 is an average bone in the set.

Results for the 1 kg tests are given below, in this test none of the femurs fractured. See figure 16 for the forces over time. See figure 17 for a plot of the strain distribution around the time of maximal force.

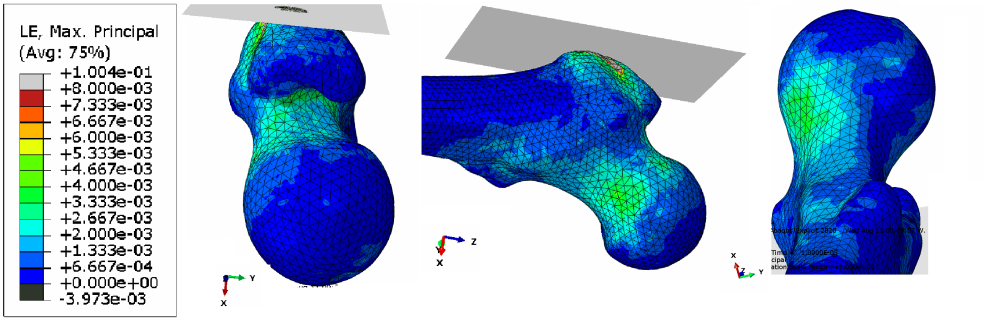

Figure 17: Strain distribution in femur 49 close to the time of the peak force was reached.

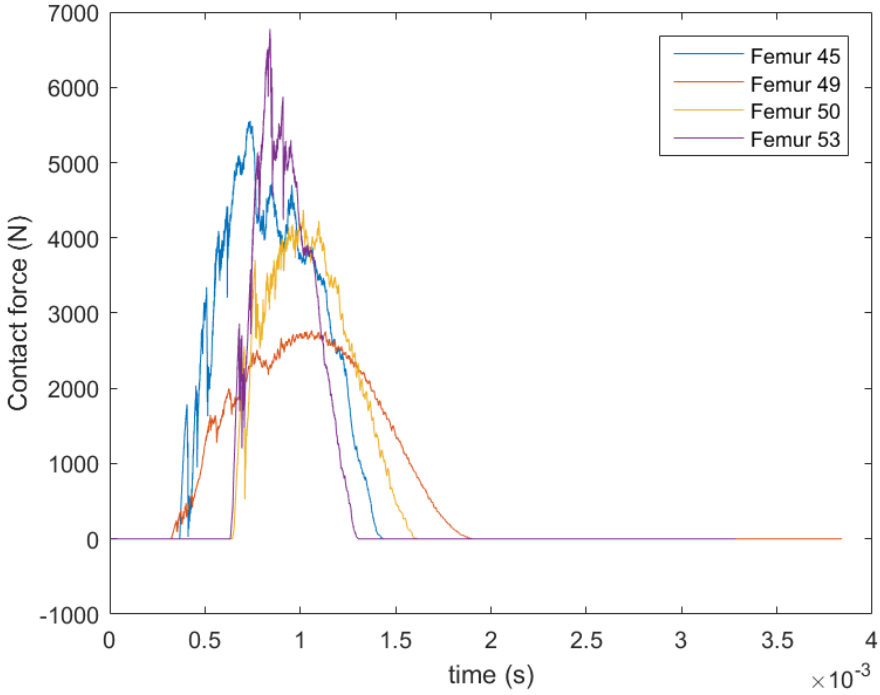

Figure 16: Contact force between the rigid fixed plane and the femur in the simulations of femurs 45, 49, 50, and 53 during the low mass tests. The horizontal axis is time in s and vertical is force in N.

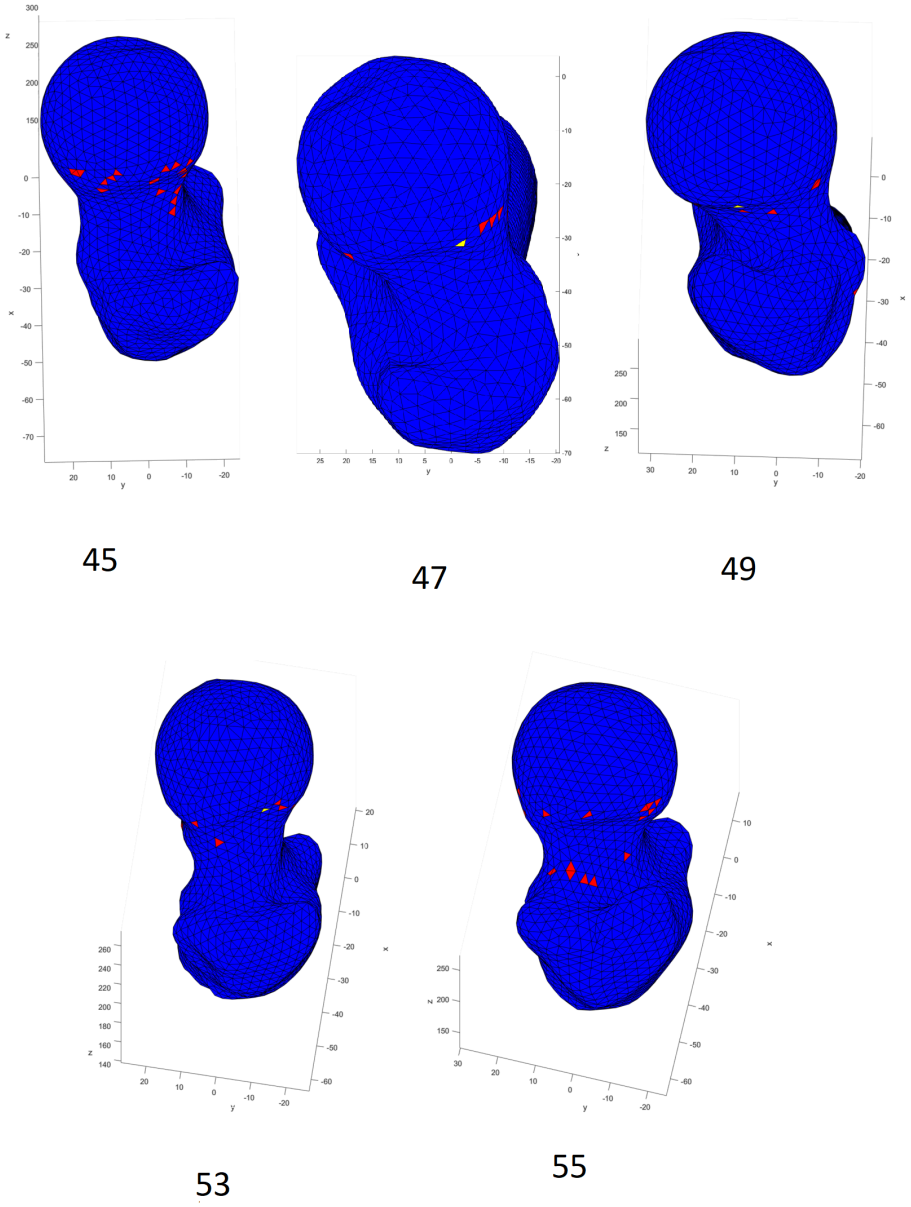

Figure 18: The fractured elements in the longer simulation for femurs 45, 47, 49, 53 and 55. The initially fractured elements are highlighted in red.

7.1 Data Analysis

The fracture force from the experimental tests and from the dynamic simulations plotted against one another can be seen in figure 19. Fitting a linear function to this by linear regression gives $y = 1.627x + 1154$ with $R^2 = 0.9304$.

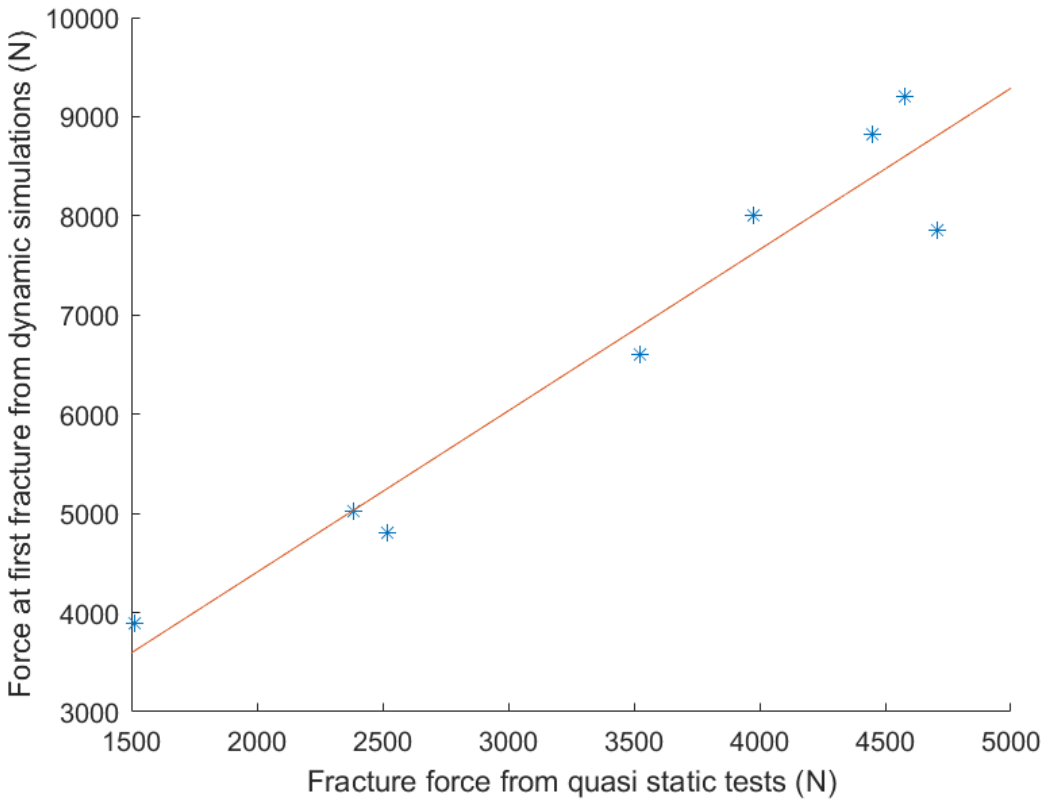

Figure 19: The fracture force from the tests and from the dynamic simulations are the dots, the line is a linear function fitted to the data by linear regression.

The peak forces from the quasi-static experimental mechanical tests were converted into expected fracture forces in a dynamic fall using equation 1 from Jazinizadeh et al. The values obtained are reported in table 4 along with the precentual difference between the fracture forces from the dynamic simulations, found in table 2, and these predicted values. For 5 of the femurs the force at fracture from the simulation was within 12% of the value expected from equation 1. The three fe-

murs where the errors were larger, between 24.1% and 36.1%, were 46, 49 and 54. These are the three weakest femurs in the set.

Table 4: Fracture force for each femur as predicted by equation 1 and how it compares to the values from the simulations in table 2 showing how the percentual difference between the predicted and simulated values.

Femur	Predicted fracture force (N)	Simulated by predicted fracture force
45	7598	+5.7%
46	6627	-24.1%
47	7888	+11.8%
49	6097	-36.1%
50	8514	+8.2%
53	8043	-2.3%
54	6710	-28.5%
55	7322	-9.8%

8 Discussion

The purpose of this project was to create a subject specific dynamic FE modeling procedure for a femurs impact with the ground. This purpose has been fulfilled in that such a modeling procedure simulating a sideways fall on the hip has been created and tested.

Overall the model seems to capture the mechanical properties of the femur and its fall and impact with the ground well. All the femur models fractured during the simulations when the entire mass of the body was applied to the femoral head. This makes sense since this models a scenario wherein the femur hits the ground without any soft tissue to absorb any energy and the amount of mass the femur must hit stop at once is likely overestimated. The kinetic energy even the strongest femur, number 50, must absorb during this fall is about 462 Nm, see table 3, which is far more than the $23.25Nm$ that was required to fracture it in Grassi et al, see table 1 [22].

The fracture force in the dynamic fall simulation was greater than what was required to fracture the femur during quasi-static testing. The femurs that proved stronger during testing also had higher contact forces at time of fracture as can be seen looking at figure 19. Comparing the fracture force expected of the femur based on equation 1 to the simulated values, most values agree fairly well with 5 of 8 bones having a fracture force within 12% of what one would expect. The exceptions to this are the weaker bones such as 49 and 46. This can be explained by the study in which this relation was found including no bones as weak as those. The worst case, femur 49, had an aBMD of 0.429 g/cm^2 while the lowest aBMD of any femur in Jazinizadeh et al was 0.759 g/cm^2.

The number of fractured elements in the simulations that ended 1000 time steps after first fracture, see table 2, seems to have little to do with the strength of the bone. Despite the fact that one might expect the size of the fracture to have some relationship with the properties of the femur or its fall there is no clear relationship between this and any other metric presented here. This may simply be because the simulations ended too soon for the percentage of fractured elements to be meaningful.

The strain distributions in figure 8 do look reasonable since, for the fractureable elements the principal strain is largest in the neck of the femur as one would expect. Looking at the figures 10 to 15 one can observe that the largest strains tend to later occur on the lateral side of the femoral neck. This seems reasonable since the places where the femur already starts yielding or fracturing should the yield further due to the decreased stiffness in those areas. The lateral femoral neck is also where all the fractures occurred when the femurs were tested and thus where one would expect them to occur during a fall. As can be seen in figures 6 and 7 this is also where most fractures occurred in the simulations. No fractures seem to have occurred in completely unexpected locations such as the shaft and by the definition of the model none occurred on the femoral head or greater trochanter. However most of the initial fractures occurred at the base of the femoral head rather than further down the lateral neck towards the greater trochanter as would be expected given that fracture locations in a sideways fall tend to happen close to where they occurred under quasi static loading. This is most likely due to problems estimating the stiffness in that region due to the thin cortical bone causing partial volume effect. The quasi static simulations ran into the same problem; therefore, a minimum stiffness of 2500 MPa was assigned to the surface elements of the quasi-static models. Applying this minimum density in the quasi static simulations solved the problem without overestimating the peak

force. This correction was not applied to the models presented in this thesis. This problem is therefore likely solvable by introducing either a minimum stiffness of the surface elements as was done there or increasing the stiffness of the elements in that specific area. It should also be noted that in three of the cases where the femur fractured in the wrong location it also fractured in the expected location later in the simulation which supports the idea that the problem is the stiffness close to the femoral head being underestimated. It can also be noted that the strain distributions in the low mass models also show higher strains present in the lateral and medial neck than elsewhere, see figure 17. The lack of fractures also make sense considering the low energies involved. The low mass models show that the model probably does not seem to greatly overestimate the strains that would occur during the impact since they did not fracture.

The model in question however has two primary limitations. The first of these limitations is that the mass placed on the femoral head to approximate a body is most likely overestimated. During a real fall it is unlikely that the femoral head would have to bear the entire mass of the body simultaneously, this most likely leads to the forces a real femur would experience during a sideways fall being overestimated. The second limitation is that there is no soft tissue in the model, since soft tissue plays an important role in absorbing energy during a sideways fall this will again lead to the forces on the femur being overestimated in the model compared to a real life fall. As an example of the size of the error, since soft tissue absorbs about 19 Nm per millimeter of thickness even 5 mm of soft tissue would have removed almost $\frac{1}{3}$ of the energy of the fall for femur 54 as well as reducing the peak force. Another problem introduced by the lack of soft tissue was that it became necessary to assume that the elements on the greater trochanter could not fracture. While this assumption should not be a large problem since fractures usually do not happen there anyway. however this assumption might not be needed in a true to life model. As can be seen in many figures, such as figures 10 to 15, in the result section the strains in the part of the bone that connected to the ground were often larger than the ones in the femoral neck which may not have been the case if there was soft tissue to spread out the impact. Removing these limitations would require more information on the subjects than was available during this project since neither the soft tissue distribution nor fall dynamics of these people were known. A third limitation is that the initial position of the femur has little actual known justification. This is most likely not a large problem however since it has been used to represent sideways falls since 1957, has produced good results and is widely adopted in the biomechanics community

[22]. It is also the configuration under which the femurs modeled in this project have previously been tested and modeled, hence why it was used here. A fourth limitation is that the yield and fracture strains as well as the relationship between strain rate and tangent stiffness were taken from experimental studies which used relatively low strain rates. Since the fracture and yield properties of bone are known to be strain rate dependent these values can't necessarily be assumed to be a good model yield and fracture strain during an impact where much higher strain rates may occur.

For the practical use of a model like this the simulations needing to stop because of the deformation speed to wave speed exceeding 1 is concerning. But it seems likely that this problem might be avoided in a more realistic model since there the deformation speed would be lower due to the reduction of the forces on the femur likely to be caused by the soft tissue and lower mass on the femoral head. No such error occurred in the simulations where the mass had been reduced. This likely means that while it may be able to simulate a fall on the side it probably could not be easily extended to model a situation giving rise to much larger deformation speeds such as a collision with a car or train. This is not a large loss since the model was never meant to model high impact situations in the first place.

8.1 Conclusion and Further Work

In conclusion the current model as presented here correctly models the femurs, their impact with the ground and deformation. The only real problem being the likely solvable issue of the femoral head being to fragile. The creation of the subject specific dynamic model from CT images does not require significantly more effort than creating a quasi-static one.

The next step in developing this model further is likely to make it more true to life. Further work on these models would be to add soft tissue to the model or otherwise account for its existence. The model for the soft tissue most likely does not need to be as detailed as that of the bone. For example since what happens to the soft tissue is largely uninteresting apart from the way it softens the fall for the femur including any way for the tissue to break is likely excessive. Modeling the soft tissue based on CT images is preferable if possible since part of the point of using FE modeling is the ability to take very detailed information about the patient into account. However one might be able to create a decent model of the soft tissue from information such as the subjects BMI and sex rather than creating it from CT images. Adding soft tissue would come with the disadvantage of most likely

slowing down the simulations, so making the soft tissue more detailed would need to be weighed against the need for decent performance. Better knowledge of the actual kinematics of a sideways fall would also help make the model more realistic, the primary such problem at current being the lack of a good way to model the mass of the body falling on the femoral head. Before being used for anything the model would also need to be tested against experiments. Since this model already runs slower than the quasi-static one it may be necessary to speed up the simulations if additional features such as soft tissue are to be added. If the model is to be used to predict the fracture risk of elderly patients it cannot reasonably require a whole day or more for each patient.

Solving the first and third limitations would require finding good values of the mass placed on the femoral head and good initial conditions for the model. Doing this would require more information about the kinematics of the fall, this could for example be acquired by modeling the subject falling on their side and then using values from that model as parameters in this one.

8.2 Ethics

This project used CT-images obtained from 12 cadavers previously used by Kok et al. These femurs were obtained at Kuopio University Hospital in Finland with permission from the Finnish National Authority for Medicolegal Affairs (TEO, 5783/04/044/07) [5,22]. No other samples were used. Further tests of this modeling procedure or of future models based on it would likely require new samples at some point, both for CT images and possibly for mechanical tests. The ethics and potential benefits of this would of course need to be considered then. Using existing CT scans and data to the greatest possible extent would likely be beneficial to maximize the usefulness of each test subject.

While this modeling procedure is not yet ready for clinical implementation, it could be useful for such in the future after further work. The ability to better predict a persons risk of hip fracture could be beneficial both to the health of the patients in question. Being able to predict who is at risk for a fractured femur, and thus take preventative measures in time, would also benefit society at large by reducing the burden placed on the healthcare system by such fractures. In use on a living person the benefits of creating a model of their femur would need to be weighed against the risk of exposing them to x-radiation. Creating a model of a healthy 20 year old's femur, for example, would likely have no benefit since there is no reason to believe he would be at any risk of a femur fracture.

9 References

1. Johnell, O., Kanis, J.A. An estimate of the worldwide prevalence and disability associated with osteoporotic fractures. Osteoporos Int 17, 1726–1733 (2006).
2. Gullberg, B., Johnell, O. Kanis, J. World-wide Projections for Hip Fracture. Osteoporos Int 7, 407–413 (1997).
3. Hernlund, E., Svedbom, A., Ivergård, M. et al. Osteoporosis in the European Union: medical management, epidemiology and economic burden. Arch Osteoporos 8, 136 (2013).
4. Lorenzo Grassi, Sami P. Väänänen, Matti Ristinmaa, Jukka S. Jurvelin, Hanna Isaksson, How accurately can subject-specific finite element models predict strains and strength of human femora? Investigation using full-field measurements,Journal of Biomechanics, Volume 49, Issue 5 (2016), Pages 802-806.
5. Joeri Kok, Lorenzo Grassi, Anna Gustafsson, Hanna Isaksson, Femoral strength and strains in sideways fall: Validation of finite element models against bilateral strain measurements, Journal of Biomechanics, Volume 122, (2021).
6. Ingmar Fleps, Pierre Guy, Stephen J Ferguson, Peter A Cripton, Benedikt Helgason, Explicit Finite Element Models Accurately Predict Subject-Specific and Velocity-Dependent Kinetics of Sideways Fall Impact, Journal of Bone and Mineral Research: Volume 34, Number 10, (2019).
7. Ingmar Fleps, Anita Fung, Pierre Guy, Stephen J. Ferguson, Benedikt Helgason, Peter A. Cripton, Subject-specific ex vivo simulations for hip fracture risk assessment in sideways falls, Bone, Volume 125, (2019), Pages 36-45.
8. `https://commons.wikimedia.org/wiki/File:Femur_-_anterior_view2.png`, This image file is licensed under the Creative Commons Attribution-Share Alike 2.1 Japan license. The image was originaly created from models availiable on `http://lifesciencedb.jp`. last accessed on 5/08/2021.
9. S. Jacob, Human Anatomy, Churchill Livingstone, 2008, Pages 135-179, ISBN 9780443103735
10. Abaqus Documentation, `https://abaqus-docs.mit.edu/2017/English/SIMACAEANLRefMap/simaanl-c-expdynamic.htm`, last accessed on 5/08/2021.
11.Klaus-Jürgen Bathe, Finite Element Procedures, Prentice Hall, New Jearsy, (1996).
12. Pasco, J.A., Seeman, E., Henry, M.J. et al. The population burden of fractures originates in women with osteopenia, not osteoporosis. Osteoporos Int 17, 1404–1409 (2006).
13. Bouxsein, M.L. Biomechanics of osteoporotic fractures. Clinic Rev Bone Miner Metab 4, 143–153 (2006)

14. Fjola Johannesdottir, Erica Thrall, John Muller, Tony M. Keaveny, David L. Kopperdahl, Mary L. Bouxsein, Comparison of non-invasive assessments of strength of the proximal femur, Bone, Volume 105, 2017, Pages 93-102, ISSN 8756-3282.
15. Anne M. Gilroy, Brian R. MacPherson, Lawrence M.Ross, Michael Schuenke, Udo Schumacher, Maekus Voll, Karl Wesker, Atlas of Anatomy Second Edition, Thieme Medical Publishers inc, New York, (2009).
16. Frank Linde, Peter Nørgaard, Ivan Hvid, Anders Odgaard, Kjeld Søballe, Mechanical properties of trabecular bone. Dependency on strain rate, Journal of Biomechanics, Volume 24, Issue 9, 1991, Pages 803-809, ISSN 0021-9290.
17. Donald T. Reilly, Albert H. Burstein, Victor H. Frankel, The elastic modulus for bone, Journal of Biomechanics, Volume 7, Issue 3, 1974, Pages 271-275, ISSN 0021-9290.
18. Harun H. Bayraktar, Elise F. Morgan, Glen L. Niebur, Grayson E. Morris, Eric K. Wong, Tony M. Keaveny, Comparison of the elastic and yield properties of human femoral trabecular and cortical bone tissue, Journal of Biomechanics, Volume 37, Issue 1, 2004, Pages 27-35, ISSN 0021-9290.
19. Enrico Schileo, Enrico Dall'Ara, Fulvia Taddei, Andrea Malandrino, Tom Schotkamp, Massimiliano Baleani, Marco Viceconti, An accurate estimation of bone density improves the accuracy of subject-specific finite element models, Journal of Biomechanics, Volume 41, Issue 11, 2008, Pages 2483-2491, ISSN 0021-9290.
20. Elise F. Morgan, Harun H. Bayraktar, Tony M. Keaveny, Trabecular bone modulus–density relationships depend on anatomic site, Journal of Biomechanics, Volume 36, Issue 7, 2003, Pages 897-904, ISSN 0021-9290.
21. Urban Lindgren, Olle Svensson, Ortopedi,Almqvist Wiksell Medicin/Liber, Stockholm, 1996.
22. Lorenzo Grassi, Joeri Kok, Anna Gustafsson, Yi Zheng, Sami P. Väänänen, Jukka S. Jurvelin, Hanna Isaksson, Elucidating failure mechanisms in human femurs during a fall to the side using bilateral digital image correlation, Journal of Biomechanics, Volume 106, 2020, 109826, ISSN 0021-9290.
23. S.N. Robinovitch, T.A. McMahon, W.C. Hayes, Force attenuation in trochanteric soft tissues during impact from a fall, J. Orthop. Res., 13 (1995), pp. 956-962.
24. Taddei F, Schileo E, Helgason B, Cristofolini L, Viceconti M. The material mapping strategy influences the accuracy of CT-based finite element models of bones: an evaluation against experimental measurements. Med Eng Phys. 2007 Nov;29(9):973-9.
25. Fatemeh Jazinizadeh, Hojjat Mohammadi, Cheryl E. Quenneville, Comparing

the fracture limits of the proximal femur under impact and quasi-static conditions in simulation of a sideways fall, Journal of the Mechanical Behavior of Biomedical Materials, Volume 103, 2020, 103593, ISSN 1751-6161,
26. Morgan EF, Unnikrisnan GU, Hussein AI. Bone Mechanical Properties in Healthy and Diseased States. Annu Rev Biomed Eng. 2018;20:119-143. doi:10.1146/annurev-bioeng-062117-121139
27. Hansen U, Zioupos P, Simpson R, Currey J. D, Hynd D, The Effect of Strain Rate on the Mechanical Properties of Human Cortical Bone, ASME. J Biomech Eng. February 2008; 130.